Handling uncertainties with affine arithmetic and probabilistic OPF for increased utilisation of overhead transmission lines

Handling Uncertainties with Affine Arithmetic and Probabilistic OPF for Increased Utilisation of Overhead Transmission Lines

Duo Fang[1], Mingzhe Zou[1], Guido Coletta[2], Alfredo Vaccaro[2], Sasa Z. Djokic[1]

[1] School of Engineering, the University of Edinburgh, Scotland, UK

[2] Department of Engineering, University of Sannio, Italy

Abstract

Large-scale integration of variable and unpredictable renewable-based generation systems poses significant challenges to the secure and reliable operation of transmission networks. Application of dynamic thermal rating (DTR) allows for a higher utilisation of transmission lines and effectively avoids high-cost upgrading and/or reinforcing of transmission system infrastructure. In order to efficiently handle ranges of uncertainties introduced by the variations of both wind energy sources and system loads, this paper introduces a novel optimization model, which combines affine arithmetic (AA) and probabilistic optimal power flow (P-OPF) for DTR-based analysis of transmission networks. The proposed method allows for the improved analysis of underlying uncertainties on the supply, transmission and demand sides, which are expressed in the form of probability distributions (e.g. for wind speeds, wind directions, wind power generation and demand variations) and related interval values. The paper presents a combined AA-P-OPF method, which can provide important information to transmission system operators for evaluating the trade-off between security and costs at a planning stage, as well as for selecting optimal controls at operational stage. The AA-P-OPF methodology is illustrated for a day-ahead planning, using a case study of a real transmission network and a medium size test distribution network.

Keywords: Affine arithmetic; dynamic thermal rating; Monte Carlo simulation; optimal operation; optimal power flow; uncertainty.

Nomenclature

Indices		
N	Set of bus numbers	
L	Set of line numbers	
l	Transmission line number	
k, m	Bus numbers, in terms of *from* and *to* ends of line l	
n	Bus number	
s	Number of Markov Chain model states	
w	Wind farm number	
Parameters		
b'_l	Total shunt susceptance of line l	$p.u.$
y'_l	Total admittance of line l	$p.u.$
$\underline{P_{Gw}}$	Lower bound of supplied active power from the w^{th} wind farm	MW
$\bar{P}_{Gw}$	Upper bound of supplied active power from the w^{th} wind farm	MW
$\overline{s_l}$	Thermal limit of transmission line l	MVA
$\underline{V_k}$	Lower bound of voltage magnitude at bus k	$p.u.$
$\bar{V}_k$	Upper bound of voltage magnitude at bus k	$p.u.$
$\mathbf{P}$	Markov Chain transition probability matrix	
$\mathbf{C}$	Cumulative Markov Chain transition probability matrix	
$\boldsymbol{\rho_g}$	Matrix of linear correlation parameters	
Variables		
P_{curtw}	Active power curtailment for the w^{th} wind farm	MW
P_{netk}	Active power injected from the grid at bus k	MW
Q_{netk}	Reactive power injected from the grid at bus k	$MVAr$
P_{Gw}	Active power injected from the w^{th} wind farm	MW
Q_{Gw}	Reactive power injected from the w^{th} wind farm	$MVAr$
P_{Dk}	Active power demand of the load connected at bus k	MW
Q_{Dk}	Reactive power demand of the load connected at bus k	$MVAr$
P_{fl}	Active power injected into line l at its *from* end	MW
Q_{fl}	Reactive power injected into line l at its *from* end	$MVAr$
P_{tl}	Active power injected into line l at its *to* end	MW
Q_{tl}	Reactive power injected into line l at its *to* end	$MVAr$
V_k	Voltage at bus k	$p.u.$
V_m	Voltage at bus m	$p.u.$
q_c	Convection heat loss rate	W/m
q_r	Radiated heat loss rate	W/m
q_s	Solar heat gain	W/m
$R(T_c)$	Resistance of conductor	Ω/m
$\widetilde{P_{GW}}$	Affine upper bound of supplied active power from the w^{th} wind farm	MW
$\widetilde{P_{Dk}}$	Affine active power demand of the load connected at bus k	MW

$\widetilde{V_w}$	Affine wind speed	m/s
$\tilde{\phi}$	Affine wind attacking angle	$degree$
$\widetilde{I_{max}}$	Affine line thermal rating	A
X, Y	Random variables	
Q	Uncorrelated sample vector	
Y	Correlated sample vector	
Functions		
$F(\cdot)$	Marginal distribution	
$C(\cdot)$	Copula function	
$\Phi(\cdot)$	CDF of Gaussian distribution	

1. Introduction

Significantly increased penetration levels of various renewable energy sources, such as wind and photovoltaics (PV) systems, have introduced a range of new challenges for network operation and control [1]-[2], as these renewable-based generation systems are both highly variable and unpredictable, so therefore cannot be dispatched as the conventional generation plants. In addition, large wind and PV farms are typically located farther away from load centres, requiring sufficient capacities of interconnecting transmission networks. Application of dynamic thermal rating (DTR) effectively avoids costly upgrading or reinforcing of transmission system infrastructure, as it allows for a higher utilisation of transmission network components than if their static thermal ratings (STR) are used. Accordingly, the DTR analysis uses thermal models of network components (e.g. overhead lines, OHL) to assess variations in their available capacities, based on the forecasted, or real-time monitored, loading and ambient conditions.

Three most-commonly used models for assessing conductor surface temperature of transmission OHLs are given in: IEC 61597, [3], IEEE Std 738-2006, [4] and CIGRE Working Group 22.12 Report, [5]. In this paper, model from [4] is used to determine OHL thermal rating, while [6] presents a comparison of these models. Previous work has shown that application of DTR can increase thermal loading of transmission lines by 5% - 15%, [7], and in that way release network capacity for connecting higher number of generation

units and supplying more loads, [8], [9], [10]. Implementation of DTR models for optimal power flow (OPF) analysis of networks with wind-based generation is presented in [11] and [12].

Building on the previous work, this paper considers a transmission OHL connecting a large wind farm, when there are uncertainties in the wind farm outputs due to inherently stochastic variations of wind speeds and wind directions, which will additionally impact uncertainties in the estimated DTR values. These uncertainties in the generation and transmission systems are considered together with the variations in the connected system loads, i.e. uncertainties on the demand side.

A number of probabilistic optimal dispatch problems are solved by numerical methods, such as Gram-Charlier method [13], which derives probability distribution functions (PDFs) from the statistical data of state variables. Analytical approaches include: convolution methods [14], chance-constrained programming [15], point estimate methods [16], etc. However, these approaches require approximations and are often strict regarding the PDF formulations of statistic variables. Recently, some new approaches have been applied to OPF analysis, such as interval analysis [17], fuzzy theory [18] and affine arithmetic [19].

For example, an affine arithmetic (AA) based numerical approach is applied in [19] to solve OPF problems with interval uncertainties, showing how internal errors caused by truncations and approximations can be taken into account in solutions with accurate output result intervals. To resolve issues of such AA approaches with too wide solution ranges, typically manifested in the low probabilities around maximum and minimum interval values, modern trends in AA-applications combine probabilistic and AA approaches, e.g. [20] and [21], where noise symbols are represented in the form of P-

boxes (i.e. generic probabilistic functions) and classified into independent group and group with unknown dependencies based on the estimated or assumed probability distributions of interval values. Although this approach allows to efficiently follow propagation of uncertainties through the computational process, it does not provide evaluation of the confidence levels and related risks associated with the solutions.

In order to efficiently handle a possibly large range of uncertainties introduced into power system by the variations of its generation, transmission and demand sides, this paper introduces a novel optimization model, which combines AA and probabilistic optimal power flow (P-OPF) for a DTR-based analysis of transmission networks. The uncertainties in bus power injections, including wind generation and load, as well as in DTR limits, are initially formulated as interval values, obtained from time series generated using a second-order Markov Chain model and Copula function. Probabilistic OPF is solved first with the AA approach, using Min-Max intervals of optimal objective function values, in order to identify optimal dispatch solutions. As mentioned, these AA interval solutions are usually too conservative, as they include all possible values of uncertain variables, regardless of their actual probabilities. Therefore, this paper uses Monte Carlo Simulations (MCS') for evaluation of probabilities and uncertainties in input values (and risks in output values), based on the methods developed in [22]. This allows to specify related uncertainties and risks with suitable confidence levels by considering corresponding AA-intervals and P-OPF solutions, i.e. to combine them into the presented AA-P-OPF method, which is illustrated on a case study of a real transmission network, as well as on a case study of a 33-bus medium-size distribution system, for a day-ahead planning studies.

The main contributions of the paper are:

- A novel approach is proposed for analysing wind speed, wind direction and load profile time series, which is specifically aimed at evaluating impact of their ranges of variations and uncertainties on the correlated power outputs of WFs and DTR of OHLs for the analysis of operational network performance.
- A novel AA-P-OPF method is presented, combining affine arithmetic and probabilistic optimal power flow analysis for significantly reduced computational times and for specifying confidence level in obtained solution ranges.
- Thermal model of overhead lines, based on the DTR analysis, is included into the OPF analysis of system capacity for evaluating operation of networks with high penetration of wind-based generation systems in terms of low-risk wind curtailment strategies.

2. Problem Definition

2.1 Wind Power Curtailment Minimization

For a given power network $G(N, L)$, where $N = \{1, \dots n\}$ and $L \subseteq N \times N$ represent sets of buses and branches (including transmission lines and transformers), respectively, and where for each branch $l \in L$, k and m represent *from* and *to* line ends (connecting buses), denoted as $l = (k, m)$, the AC OPF problem for minimizing wind curtailment can be written as:

$$\min \sum_{w \in W} P_{curtw}^2 \tag{1}$$

where P_{curtw} is the wind power curtailment for the w^{th} wind farm (WF).

Subject to:

- Power balance equations:

$$P_{netk} + \sum_{w \in W_k} P_{Gw} - P_{Dk} = \sum_{l=(k,m) \in L} P_{fl} + \sum_{l=(m,k) \in L} P_{tl} \quad \forall k \in N \tag{2}$$

$$Q_{netk} + \sum_{w \in W_k} Q_{Gw} - Q_{Dk} = \sum_{l=(k,m) \in L} Q_{fl} + \sum_{l=(m,k) \in L} Q_{tl} \quad \forall k \in N \tag{3}$$

where at every bus k: P_{netk} and Q_{netk} are active and reactive power from the grid at bus k (For any buses which are not slack bus, $P_{netk} = 0, Q_{netk} = 0$), P_{Gw} and Q_{Gw} are active and reactive power injected by the w^{th} WF, and P_{D_k} and Q_{Dk} are active and reactive power demands of the connected load. W_k is the subset of wind farms located at bus k.

- Line flow equations:

$$\frac{V_k}{t_l}\left[\left(\frac{jb_l'}{2} + y_l\right)V_k - y_l V_m\right]^* = P_{fl} + jQ_{fl} \quad \forall\, l = (k,m) \in L \tag{4}$$

$$V_m\left[-y_l V_k + \left(\frac{jb_l'}{2} + y_l\right)V_m\right]^* = P_{tl} + jQ_{tl} \quad \forall\, l = (k,m) \in L \tag{5}$$

where b_l' is the total shunt susceptance of line l; pairs P_{fl} and Q_{fl}, and P_{tl} and Q_{tl}, are active and reactive powers injected into line l at its *from* and *to* ends, respectively, with V_m and V_k voltages at *from* and *to* ends of line l.

- Wind farm capacities:

$$\underline{P_{Gw}} \le P_{Gw} \le \overline{P}_{Gw} \quad \forall w \in W \tag{6}$$

where $\underline{P_{Gw}}$ and $\overline{P}_{Gw}$ are upper and lower bounds of active power supplied by the w^{th} WF.

- Line thermal limits:

$$\left|P_{fl} + jQ_{fl}\right|^2 \le \overline{s_l}^2, \ \ |P_{tl} + jQ_{tl}|^2 \le \overline{s_l}^2 \quad \forall l \in L \tag{7}$$

where $\overline{s_l}$ is the thermal limit (i.e. capacity limit in MVA) of transmission line l.

- Bus voltage magnitude limits:

$$\underline{V_k}^2 \le |V_k|^2 \le \overline{V_k}^2 \quad \forall k \in N \tag{8}$$

where $\overline{V_k}$ and $\underline{V_k}$ are the upper and lower bounds of voltage magnitude at bus k.

- Slack bus constraint:

$$V_k = 1 + j0, \text{ for } k = \text{slack bus} \tag{9}$$

2.2 Dynamic Thermal Rating (DTR)

The DTR of an OHL, also known as real-time thermal rating, considers actual loading and weather conditions (e.g. ambient temperature, wind speed, wind direction, solar irradiance, etc.), in order to more accurately estimate OHL temperature and then evaluate available OHL capacity, [4]:

$$I_{max} = \sqrt{\frac{q_c(T_c,T_a,V_w,\phi)+q_r(T_c,T_a)-q_s}{R(T_c)}} \quad (10)$$

where q_c and q_r are convection and radiation heat loss rates (impacted by wind speed V_w, wind attacking angle ϕ and ambient temperature T_a), q_s is solar heat gain and $R(T_c)$ is resistance of conductor at temperature T_c. The DTR is included into OPF analysis by replacing $\overline{s}_l$ in (7) with $\overline{s}_{lD}$:

$$\overline{s}_{lDf} = \sqrt{3}V_k I_{maxl},\ \overline{s}_{lDt} = \sqrt{3}V_m I_{maxl} \quad \forall\, l = (k,m) \in L \quad (11)$$

2.3 Affine Arithmetic

Affine arithmetic (AA) is a self-validated numerical computation model, which is used to solve dependency problems in classical interval mathematic computations. It keeps track of the first-order correlations between input and computed output quantities [23]. Standard interval arithmetic (IA) often yields to much wider intervals than the actual (exact) ranges of the computed function, resulting in an overestimation that effectively limits the application of the IA. For instance, in chained computation, where the outputs of one step are inputs of the next step, the overestimation tends to get multiplied. This results in a cumulative error, also known as error explosion, which can be resolved by applying affine arithmetic.

Assuming that $\tilde{x}$ is a variable which is subject to uncertainties, the affine form of $\tilde{x}$ is:

$$\tilde{x} = x_o + x_1\varepsilon_1 + x_2\varepsilon_2 + \cdots + x_n\varepsilon_n \quad (12)$$

where x_o, is central value, x_i are deviations due to the i^{th} uncertainty, for which ε_i represents the noise symbol with the range $[-1,1]$. The radius of $\tilde{x}$ can be expressed by $radx = \sum_{i=1}^{n} |x_i|$. $[\underline{x}, \overline{x}]$, when the range of $\tilde{x}$ can be given as:

$$\underline{x} = x_o - radx, \overline{x} = x_o + radx \tag{13}$$

Affine arithmetic consists of affine and non-affine operations. For two interdependent affine forms $\tilde{x} = x_o + \sum_{i=1}^{n} x_i \varepsilon_i$ and $\tilde{y} = y_o + \sum_{i=1}^{n} y_i \varepsilon_i$, the affine form $\tilde{z}$, determined by affine combinations of $\tilde{x}$ and $\tilde{y}$, is:

$$\tilde{z} = \alpha\tilde{x} \pm \beta\tilde{y} \pm \gamma = (\alpha x_o \pm \beta y_o \pm \gamma) + \sum_{i=1}^{n} (\alpha x_i \pm \beta y_i)\varepsilon_i \tag{14}$$

where the middle point of $\tilde{z}$ is given as $z_o = \alpha x_o \pm \beta y_o \pm \gamma$ and deviation of the i^{th} uncertainty is $z_i = \alpha x_i \pm \beta y_i$. For a non-affine operation$z \leftarrow f(x, y)$, as f^* is not affine, z cannot be expressed exactly by affine combinations of noise symbols ε_i. Affine approximation is necessary in this case and an extra term $z_k \varepsilon_k$ should be introduced.

$$\tilde{z} = f^a(\varepsilon_1, \dots, \varepsilon_n) + z_k \varepsilon_k \tag{15}$$

where $f^a(\varepsilon_1, \dots, \varepsilon_n) = \alpha\tilde{x} + \beta\tilde{y} + \gamma$. The optimal values of α, β, γ and $z_k$to minimize approximation errors can be determined by Chebyshev approximations [24].

By formulating uncertain bus power injections in affine form as (16) and (17), affine forms of the other state variables can be derived according to power balance equations [19], [25], [26]. For WF maximum supplied power:

$$\widetilde{\overline{P_{GW}}} = \overline{P_{GWo}} + \overline{P_{GW}}\varepsilon_w \quad \forall w \in W \tag{16}$$

while for load:

$$\widetilde{P_{Dk}} = P_{Dko} + P_{Dk}\varepsilon_k, \quad \widetilde{Q_{Dk}} = Q_{Dko} + Q_{Dk}\varepsilon_k \quad \forall k \in N \tag{17}$$

where each wind generation and load have different error symbols.

The affine formulation of DTR in this paper considers uncertainties in wind speeds and wind directions, as previously presented in [27], which can be respectively expressed by (18) and (19).

$$\widetilde{V_w} = V_{wo} + V_w \varepsilon_w \quad \forall w \in W \tag{18}$$

$$\tilde{\phi} = \phi_o + \phi \varepsilon_\phi \tag{19}$$

The affine form to represent DTR can be calculated as:

$$\widetilde{I_{max}} = \sqrt{\frac{\widetilde{q_c} + \widetilde{q_r} - \widetilde{q_s}}{\tilde{R}}} \tag{20}$$

with the final formulation is given by:

$$\widetilde{I_{max}} = I_{maxo} + I_{maxw} \varepsilon_w + I_{max\phi} \varepsilon_\phi \tag{21}$$

As previously discussed, AA-based analysis can take into account various sources of uncertainties and their assumed ranges during the assessment of DTR and is also efficient in terms of the required computation times. However, it can result in too wide solution ranges, where of particular concerns are low-probabilities around the minimum and maximum values. Therefore, this paper combines AA and probabilistic DTR analysis, which is discussed in the further text.

3. Time series and uncertainty analysis for wind and load profiles

3.1 Demand Modelling and Load Profile Uncertainties

For evaluation of load profile uncertainties, two 6-year demand time series, recorded as average 30-minute active powers, are used. Two uncertainty models are compared.

- Sliding window approach

Demands on weekdays and weekends are quite different and load profiles are therefore classified in two categories: weekdays (WKD) and weekends (WKE). A sliding window is implemented for each record in the active power measurements series, consisting of all recordings from the same hour of an identical category day (WKD or WKE) within ±14 days interval. For an individual WKD record, there are 21 values in the sliding window, while for every WKE record, there are 9 sliding windows entries.

The variations of recorded demands in the sliding window represent the uncertainty associated to the actual recording (i.e., centre position value in the window), which can be expressed by either maximum or minimum, or quantile points, as shown in Figure 1.

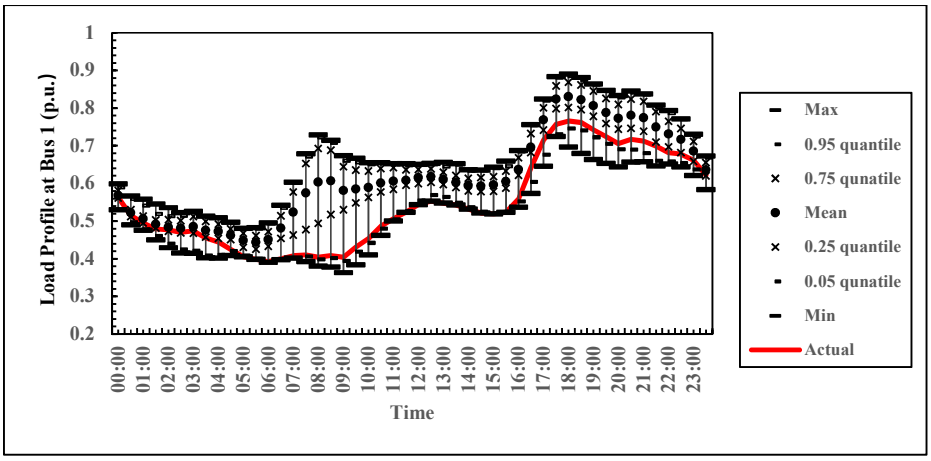

Figure 1. Evaluation of demand uncertainty with sliding window approach.

It is assumed that demand variations follow normal distribution, which is fitted by maximum likelihood estimation (MLE) method and validated by three normality tests: Jarque-Bera test (JB-test), Anderson-Darling test (AD-test) and Shapiro-Wilk test (SW-test), with 5% significance level.

- Second-order Markov Chain (MC) analysis

The second-order Markov Chain (MC) model, in which probability of transition from one state to the next state depends only on the two successive previous states, is also used to analyse variations in the WKD and WKE load profile time series:

$$\Pr(X_{n+1}=x|X_1=x_1,X_2=x_2,X_3=x_3,\ldots,X_n=x_n)=\Pr(X_{n+1}=x|X_{n-1}=x_{n-1},X_n=x_n),\ \text{if}\ \Pr(X_1=x_1,X_2=x_2,X_3=x_3,\ldots,X_n=x_n)>0 \tag{22}$$

where X_1, X_2, X_3 ... is a sequence of random variables. The recorded demand data are fuzzily approximated with a resolution of 0.5MW as:

$$\mathrm{P}_{\mathrm{new}}=\left\lfloor \frac{\mathrm{P}_{\mathrm{old}}}{0.5} \right\rfloor \times 0.5+\frac{0.5}{2} \tag{23}$$

where: P is recorded active power data, and ⌊ ⌋ is floor function. The number of MC model states is equal to the rank of the corresponding sorted active power, with transition probability matrix, $\mathbf{P}$, giving probabilities of state-to-state transfers; cumulative transition probability matrix $\mathbf{C}$ gives cumulative transfer probabilities:

$$\mathbf{P}=\begin{bmatrix} p_{111} & p_{112} & \mathrm{L} & p_{11s} \\ p_{121} & p_{122} & \mathrm{L} & p_{12s} \\ \mathrm{M} & \mathrm{M} & \mathrm{O} & \mathrm{M} \\ p_{1s1} & p_{1s2} & \mathrm{L} & p_{1ss} \\ \mathrm{M} & \mathrm{M} & \mathrm{O} & \mathrm{M} \\ p_{ss1} & p_{ss2} & \mathrm{L} & p_{sss} \end{bmatrix} \quad \mathbf{C}=\begin{bmatrix} c_{111} & c_{112} & \mathrm{L} & c_{11s} \\ c_{121} & c_{122} & \mathrm{L} & c_{12s} \\ \mathrm{M} & \mathrm{M} & \mathrm{O} & \mathrm{M} \\ c_{1s1} & c_{1s2} & \mathrm{L} & c_{1ss} \\ \mathrm{M} & \mathrm{M} & \mathrm{O} & \mathrm{M} \\ c_{ss1} & c_{ss2} & \mathrm{L} & c_{sss} \end{bmatrix} \tag{24}$$

where: s is the number of states, and p_{ijk} is the probability of transferring from state i (at $t=t-1$) and following state j (at $t=t$) to the state k (at $t=t+1$). The elements of $\mathbf{P}$ are calculated with the MLE method from [28] and elements of $\mathbf{C}$ are then calculated as $c_{ijk}=\sum_{x=1}^{k} p_{ijx}$. The empirical mean, variance, median, maximum and minimum values, as well as cumulative probability boundaries of quantiles (denoted as $(1-Q_x)$ and Q_x, where Q_x is quantile value) of transferring from states i and j are:

$$\begin{aligned} \mathrm{mean}_{ij} &= \sum_{k=1}^{s} k \times p_{ijk} \\ \mathrm{variance}_{ij} &= \sum_{k=1}^{s} p_{ijk} \times \left(k-\mathrm{mean}_{ij}\right)^2 \\ \mathrm{median}_{ij} &= k \quad s.t.\ \left|c_{ijk}-0.5\right|=\min\left(\left|c_{ijk}-0.5\right|\right), \text{where } k=\{1,\mathrm{K}\ ,s\} \end{aligned} \tag{25}$$

$$\max_{ij}=k \quad s.t. c_{ijk}=1, c_{ijk+1}=1, \mathrm{K}, c_{ijs}=1, \text{where } k=\{1, \mathrm{K}, s\}$$

$$\min_{ij}=k \quad s.t. c_{ijk}\neq 0, c_{ijk-1}=0, \mathrm{K}, c_{ij1}=0, \text{where } k=\{1, \mathrm{K}, s\}$$

$$(1-Q_x)_{ij}=k \quad s.t. \left|c_{ijk}-(1-Q_x)\right|=\min\left(\left|c_{ijk}-(1-Q_x)\right|\right), \text{where } k=\{1, \mathrm{K}, s\}$$

$$(Q_x)_{ij}=k \quad s.t. \left|c_{ijk}-Q_x\right|=\min\left(\left|c_{ijk}-Q_x\right|\right), \text{where } k=\{1, \mathrm{K}, s\}$$

For median_{ij}, if there exist multiple solutions of k, then their mean value is chosen. If $(1-Q_x)_{ij}=k$ has multiple solutions, the smallest k is selected, and for $(Q_x)_{ij}=k$, the largest k is selected, if it has more than one solution. Like in sliding window approach, variations of transfer states are fitted with normal distributions by MLE, with an example of the second-order MC model for assessing uncertainties in hourly demands shown in Figure 2 (same day as in Figure 1).

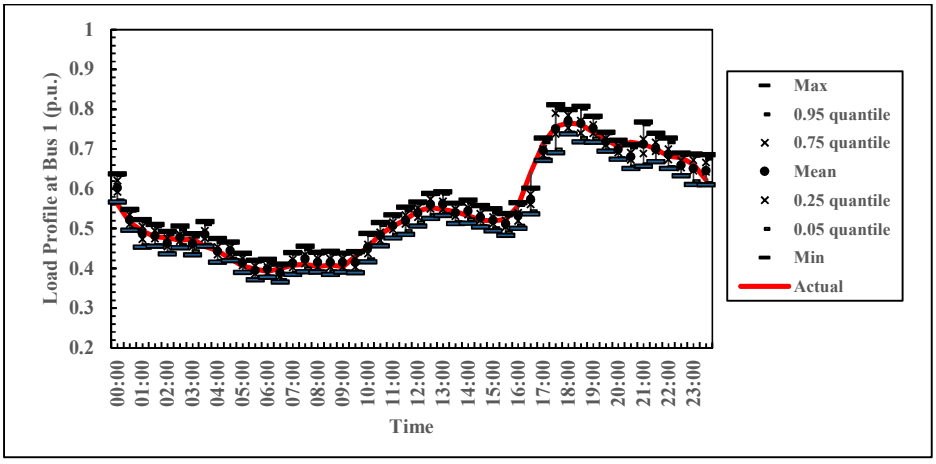

Figure 2. Demand uncertainty evaluation with the second-order MC model

As the second order MC model is based on the whole recorded dataset (annual values), where two successive previous recordings are considered as the condition for the next estimated value, the second order MC model is selected for the uncertainty analysis of load profiles.

3.2 Generated Cross-Correlated Wind Profiles

Correlated wind profiles for several WFs are generated based on Copula theory [29]-[30] and MC Model. Copula function is a multivariate PDF with uniformly distributed

marginal probability for each variable [31]. Considering a bivariate distribution, according to Sklar`s theory [32], if the marginal distributions F_X and F_Y are known, their joint distribution F_{XY} can be written as $F_{XY}(x,y)=C\left(F_X(x),F_Y(y)\right)$. If F_X and F_Y are continuous, then the Copula function C is unique.

If $F_X(x)=u$ and $F_Y(y)=v$, where u and v are respectively realisations of uniformly distributed variables U and V, $C_{UV}(u,v)=F\left(F_X^{-1}(u),F_Y^{-1}(v)\right)$ can be used to build corresponding Copula function from multivariate distribution function and multivariate Gaussian Copula is applied in this paper to analyse high-dimensional correlations between wind speeds at several WFs, as well as for transmission network OHLs.

Multivariate Gaussian Copula function has one Copula linear correlation parameter ρ_g for every bivariate dependence, so the *d*-dimensional Gaussian Copula can be written as:

$$C_g\left(u_1,u_2,\mathrm{K}\ ,u_d;\boldsymbol{\rho}_{\mathbf{g}}\right)=\Phi_{\boldsymbol{\rho}_{\mathbf{g}}}\left(\Phi^{-1}(u_1),\Phi^{-1}(u_2),\mathrm{K}\ ,\Phi^{-1}(u_d)\right) \tag{26}$$

$$c_g\left(u_1,u_2,\mathrm{K}\ ,u_d;\boldsymbol{\rho}_{\mathbf{g}}\right)=\frac{\partial^d C_g\left(u_1,u_2,\mathrm{K}\ ,u_d;\boldsymbol{\rho}_{\mathbf{g}}\right)}{\partial u_1\partial u_2\,\mathrm{K}\,\partial u_d} \tag{27}$$

$$=\left|\boldsymbol{\rho}_{\mathbf{g}}\right|^{-\frac{1}{2}}\exp\left(-\frac{1}{2}\boldsymbol{\zeta}_{\mathbf{g}}{}^{\mathrm{T}}(\boldsymbol{\rho}_{\mathbf{g}}{}^{-1}-\mathbf{I})\boldsymbol{\zeta}_{\mathbf{g}}\right)$$

$$\boldsymbol{\zeta}_{\mathbf{g}}=\left(\Phi^{-1}(u_1),\Phi^{-1}(u_2),\mathrm{K}\ ,\Phi^{-1}(u_d)\right) \tag{28}$$

This approach transforms marginal distributions into a uniform domain in [0,1] using marginal cumulative density function (CDF), and then transforms the uniform domain into a normal domain [30]. In that way, dependencies between $x_i\ (i=1,2,3,\mathrm{K}\ ,d)$ are expressed by the dependencies between their standard normal transforms. In fitting Gaussian Copula, parameter $\boldsymbol{\rho}_{\mathbf{g}}$ is again estimated using MLE method [28].

Since correlation matrix $\boldsymbol{\rho}_{\mathbf{g}}$ is a positive definite matrix, Cholesky factorisation can be applied: $\boldsymbol{\rho}_{\mathbf{g}} = \mathbf{T}\mathbf{T}^{*}$, where $\mathbf{T}$ is a lower triangular matrix and $\mathbf{T}^{*}$ is its conjugate transpose. The first step of sampling from a given Gaussian *d*-dimensional Copula is to generate *d*-dimensional variable $\mathbf{Q} = [\mathbf{q}_1, \mathbf{q}_2, \mathrm{K}, \mathbf{q}_d]$, which can be uncorrelated, and every dimension of the variable $\mathbf{q}_i$ ($i = \{1, 2, \mathrm{K}, d\}$) follows standard normal distribution. The target correlated variable $\mathbf{Y} = [\mathbf{y}_1, \mathbf{y}_2, \mathrm{K}, \mathbf{y}_d]$ can be obtained from $\mathbf{Y} = \mathbf{T}\mathbf{Q}$. Afterwards, by applying inverse standard normal distribution, $\mathbf{Y}$ can be transferred into a correlated variable in the uniform domain in $[0,1]$.

The available datasets are 3-year recordings at nine uncorrelated locations: one (L1) with synchronous/simultaneous recording of wind speed and wind direction, and eight (L2-L9) with only wind speed measurements. The synchronous wind speed and wind direction time series are used for wind profile at the OHLs. For L2-L9, MC models are fitted based on the historical data and new eight auto-correlated wind speed time series are obtained based on the transition matrices. To generate required cross-correlated wind speed time series, the target correlation matrix $\boldsymbol{\rho}_{\mathbf{g}}$ in Table I is assumed [33]:

Table I: Target correlation matrix $\boldsymbol{\rho}_{\mathbf{g}}$

	L1	L2	L3	L4	L5	L6	L7	L8	L9
L1	1	0.900	0.840	0.810	0.650	0.890	0.680	0.670	0.770
L2	0.900	1	0.930	0.940	0.830	0.910	0.850	0.850	0.860
L3	0.840	0.930	1	0.940	0.820	0.840	0.860	0.850	0.800
L4	0.810	0.940	0.940	1	0.860	0.820	0.910	0.910	0.860
L5	0.650	0.830	0.820	0.860	1	0.750	0.860	0.850	0.750
L6	0.890	0.910	0.840	0.820	0.750	1	0.790	0.790	0.880
L7	0.680	0.850	0.860	0.910	0.860	0.790	1	0.980	0.860
L8	0.670	0.850	0.850	0.910	0.850	0.790	0.980	1	0.870
L9	0.770	0.860	0.800	0.860	0.750	0.880	0.860	0.870	1

Table II shows obtained auto- and cross-correlated wind speed time series:

Table II: Calculated correlation matrix of simulation time series

	L1	L2	L3	L4	L5	L6	L7	L8	L9
L1	1	0.893	0.847	0.806	0.642	0.889	0.676	0.666	0.767
L2	0.893	1	0.928	0.939	0.824	0.903	0.841	0.847	0.859
L3	0.847	0.928	1	0.934	0.816	0.845	0.855	0.848	0.804
L4	0.806	0.939	0.934	1	0.852	0.812	0.893	0.904	0.860
L5	0.642	0.824	0.816	0.852	1	0.743	0.848	0.841	0.741
L6	0.889	0.903	0.845	0.812	0.743	1	0.790	0.786	0.874
L7	0.676	0.841	0.855	0.893	0.848	0.790	1	0.973	0.858
L8	0.666	0.847	0.848	0.904	0.841	0.786	0.973	1	0.871
L9	0.767	0.859	0.804	0.860	0.741	0.874	0.858	0.871	1

An example of the correlated daily wind profiles (generated for eight WF sites and one OHL) is illustrated in Figure 3a. The uncertainties in the wind speeds and wind directions are calculated based on the applied MC model, using approach similar to the one described in Section 3.1, which is further illustrated for WF1 in Figure 3b.

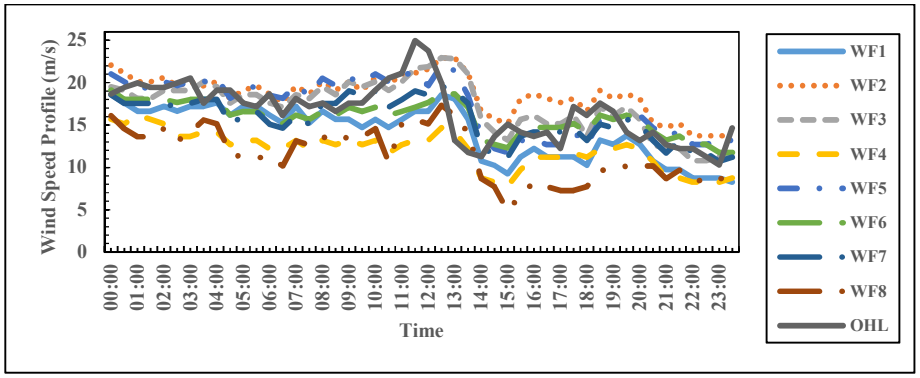

a)

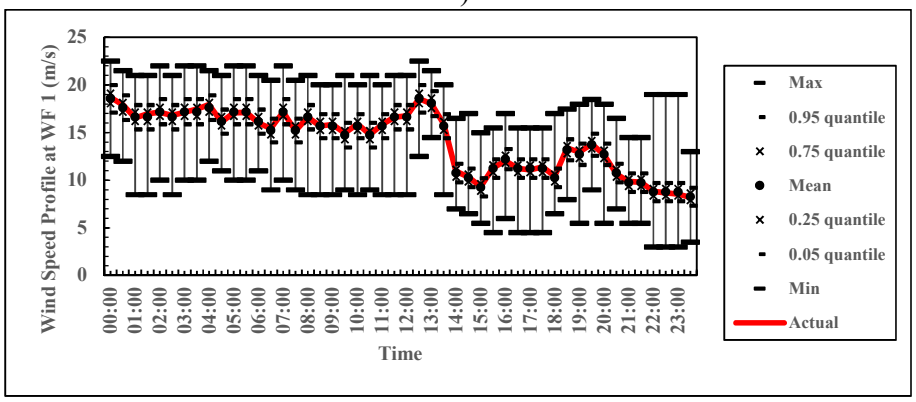

b)

Figure 3. Evaluation of wind energy resource: a) nine correlated wind speed profiles, and b) one of the corresponding wind profiles (for WF1) with identified ranges of variations/uncertainties.

4 Two Study Cases Used for Analysis

4.1 Case 1: 10-bus Network (Small Real Network)

4.1.1 Network specification

This case study is a real transmission network, Figure 4, with a high penetration of wind power, where frequent OHL congestion (i.e. overloading of OHLs in terms of their STR limits) results in wind energy curtailment. The network has 10 buses, where Bus 1 is the slack bus (connection point to HV bulk power system). There are eight wind farms, WF1 to WF8, operating with unity power factor and two bulk load supply points, L1 and L2, located at Bus 3 and Bus 10, with peak demands of 56 MW, 6 MVAr and 50 MW, 5 MVAr, respectively. All lines in network are OHLs, whose dynamic thermal ratings can be calculated according to thermal model presented in Section 2. The STR and DTR limits are implemented on all lines, which are assumed to be ACSR 'Fox' conductor type, [35]. Detailed network information can be obtained from [34].

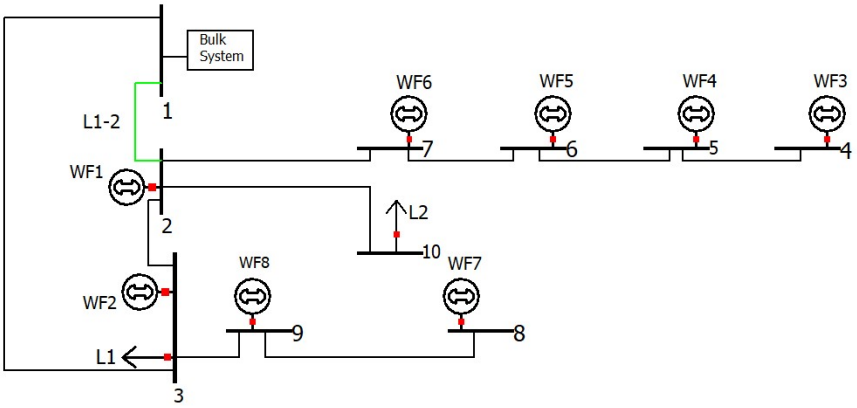

Figure 4. Configuration of the analysed network.

4.1.2 Wind profiles, load profiles and their uncertainties

Two days are selected for analysis: one in summer (6th of June) and one in winter (2nd of January), in order to evaluate seasonal variations in DTR limits. Using the methodology presented in Section 3, daily wind speed profiles for WF1-WF8, daily load profiles for L1 andL2, as well as daily wind speed and wind direction profiles for OHLs are generated for these two days, based on the available historical measurements with evaluated ranges

of uncertainties (the time step for all time series is 30 minutes). Example wind speed profiles for WF1 (Bus 2) and load profiles for L1 (Bus 3) are plotted in Figures 5 and 6, while wind speed and wind direction profiles for OHL L1-2 are plotted in Figures 7 and 8, all for the two selected days.

For a given wind speed profiles, power outputs of wind turbines (WTs) in WF can be estimated through many approaches [34]. Most common approach is the use of manufacturer power curve, which specifies the relationship between the input wind speed and WT output power. However, manufacturer power curves are obtained in controlled conditions (air-tunnels), where impact of variations in wind speeds and wind directions, WT dynamics and other site and application specific factors are not considered. In order to fully represent uncertainties in WF power outputs, probabilistic models developed in [22] and [37] are applied to estimate WF output generation profiles and their uncertainties, for generated input wind speed profiles, with Figure 8 giving an example for WF1.

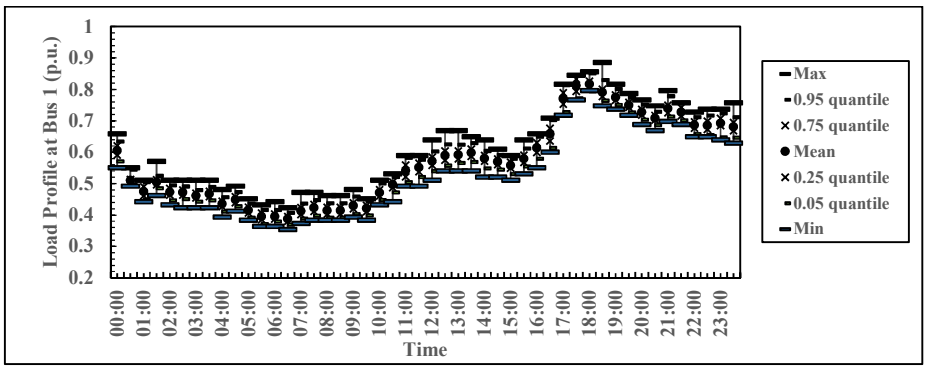

a) winter day

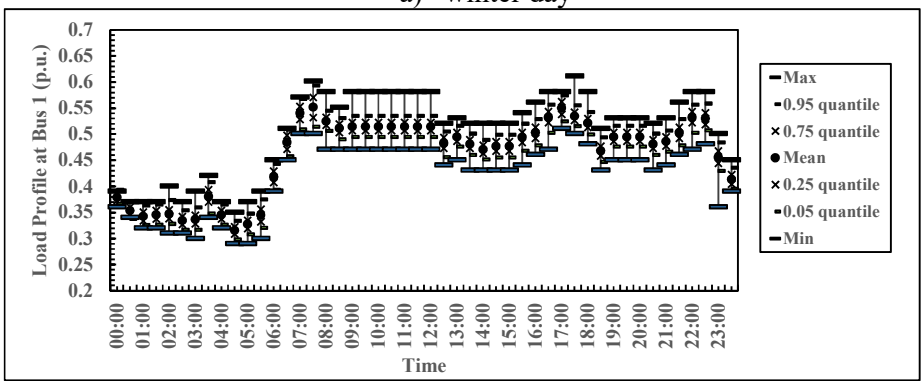

b) summer day

Figure 5. Daily load profiles and uncertainties for load L1 at Bus 3.

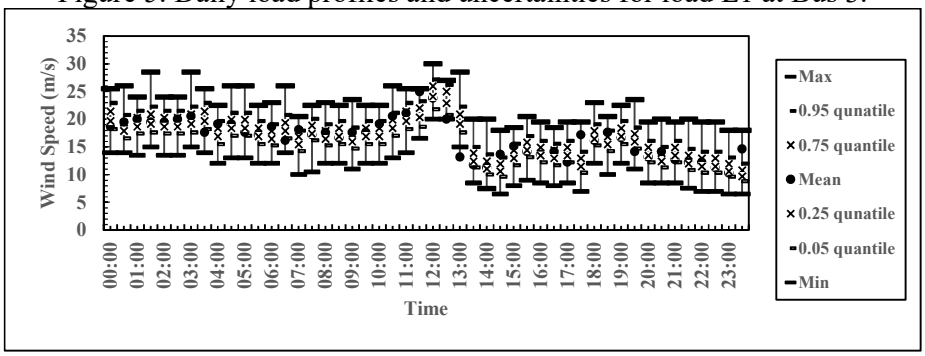

a) winter day

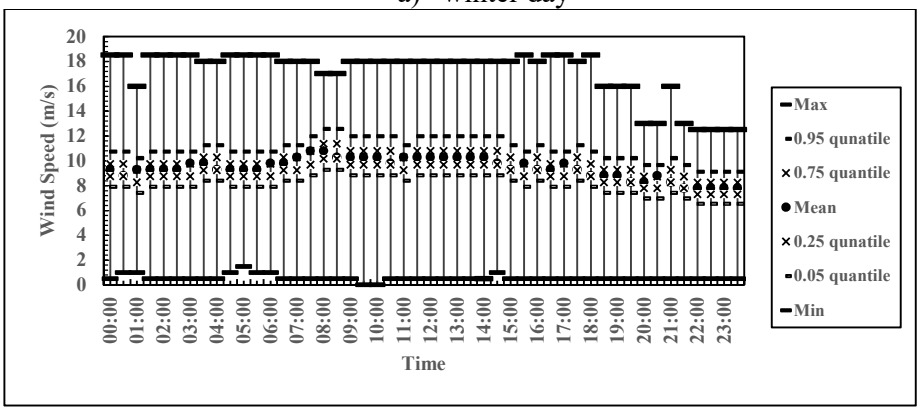

b) summer day

Figure 6. Daily wind speed profile and uncertainties at OHL L1-2.

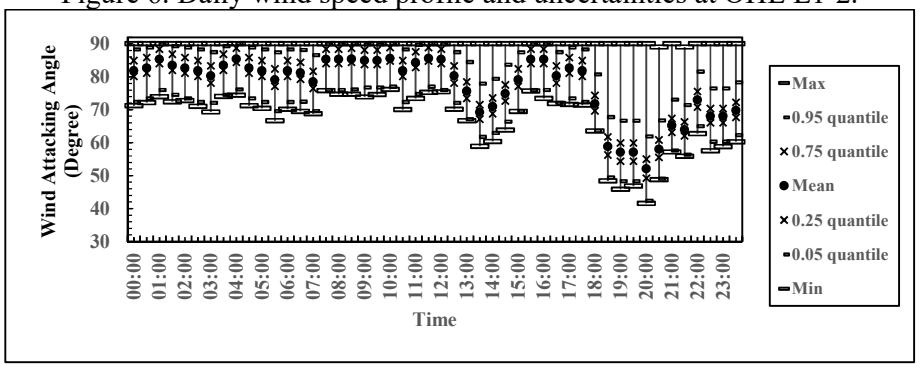

a) winter day

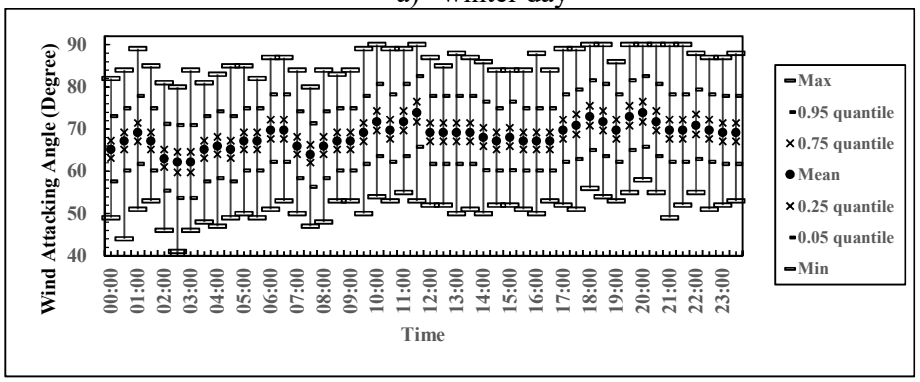

b) summer day

Figure 7. Daily wind direction (line attacking angle) and uncertainties at OHL L1-2.

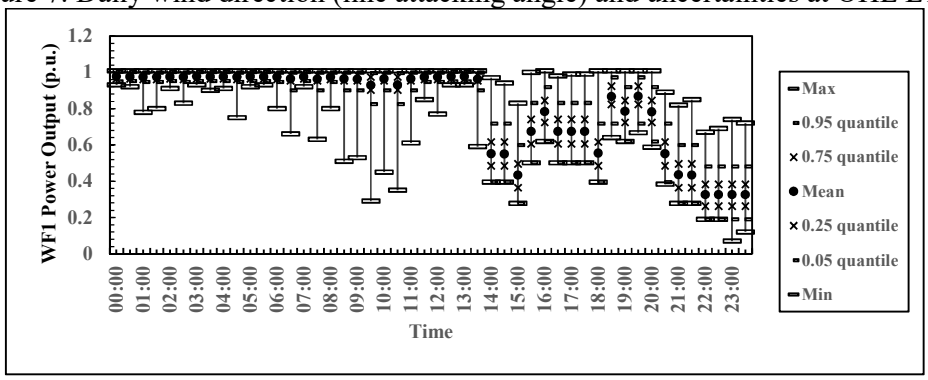

a) winter day

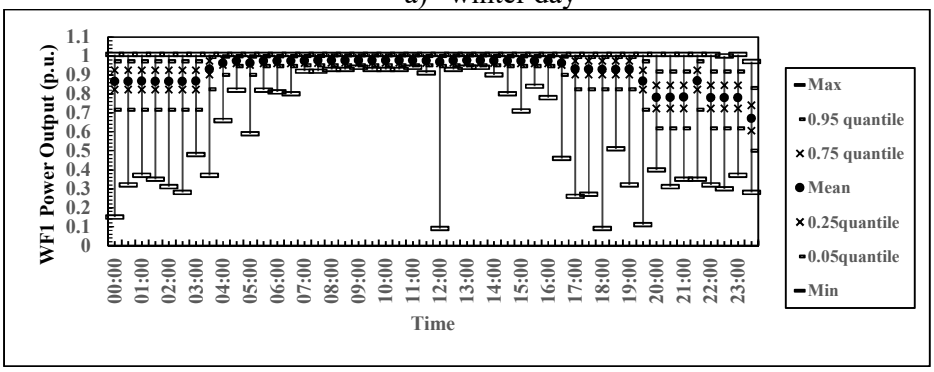

b) summer day

Figure 8. Daily power output and uncertainties for WF1.

4.1.3 Comparison between DTR and STR values

Firstly, Min-Max ranges of DTR values, corresponding to minimum and maximum wind speed and wind direction uncertainties (as in Figures 6 and 7), are used as input values in the AA-based OPF method. The evaluated upper and lower bounds of DTR values, as well as STR value, are plotted for the considered day and L1-2 in Figure 9. As the load profile is recorded with the resolution of 30 minutes, the DTR is also calculated with this resolution. The time constant of the considered OHL conductor is in the order of 10 minutes, [38] and [39], which means that the OHL will reach steady state thermal operating condition within each 30-minute period, i.e. that thermal capacitance of the OHL conductor can be neglected.

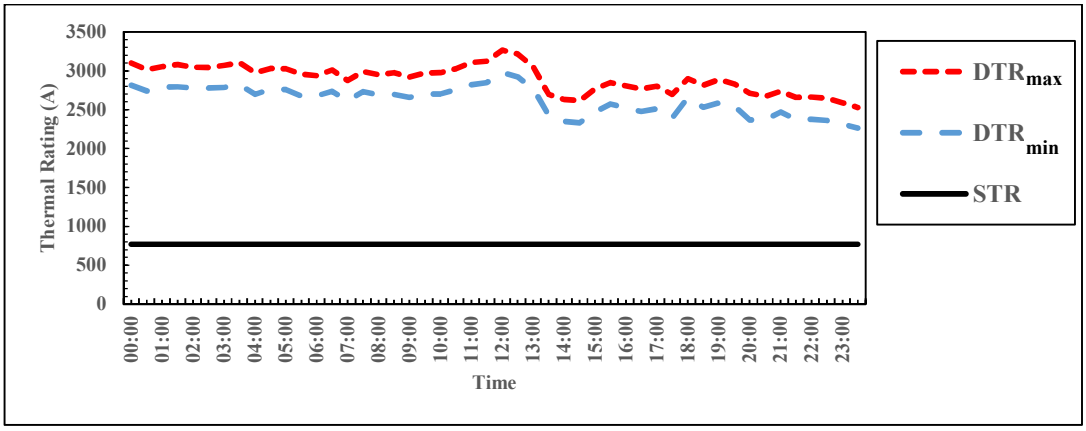

a) winter day

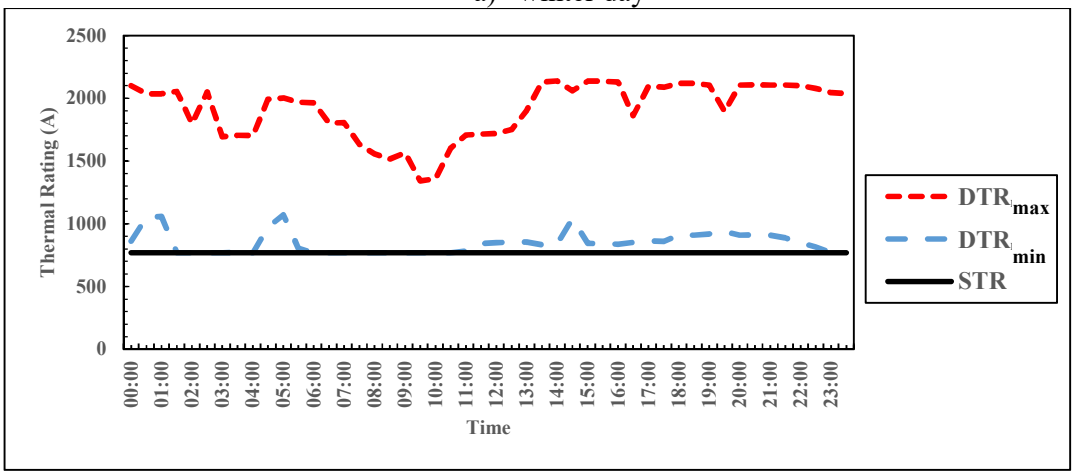

b) summer day

Figure 9. Comparison between STR and AA-OPF DTR values for L1-2.

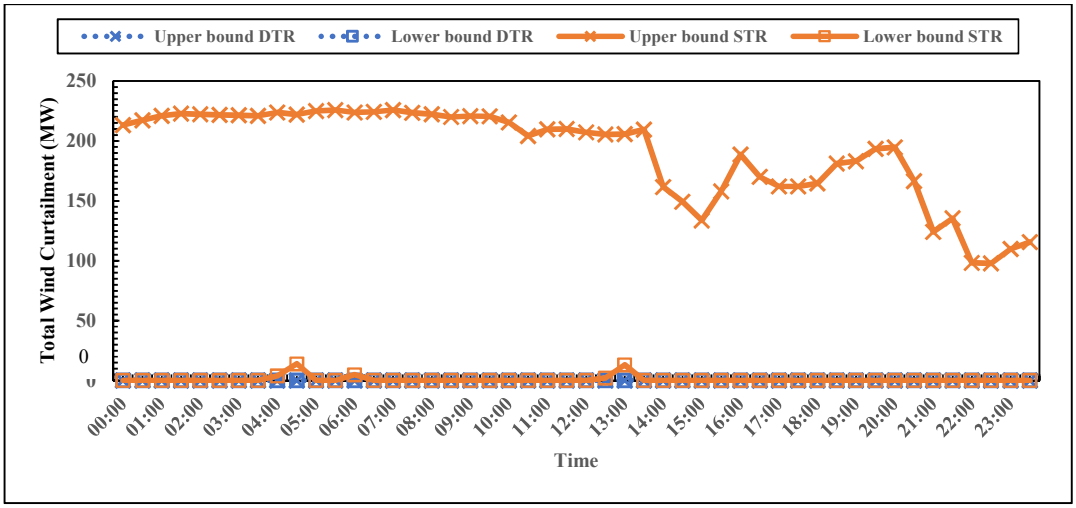

a) winter day

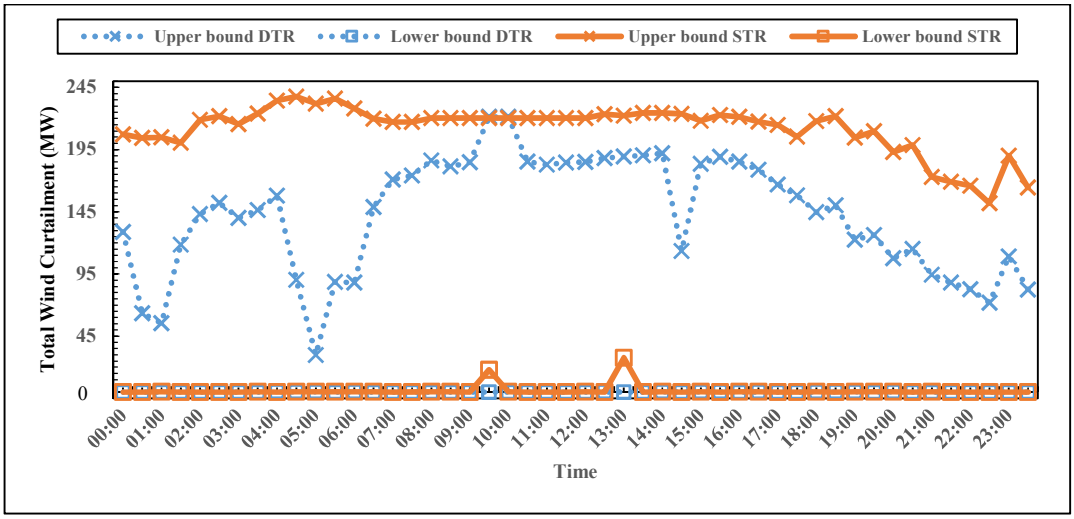

b) summer day

Figure 10. Comparison of wind curtailments with STR and AA-OPF DTR limits.

To evaluate benefits of applying DTR limits for maximising wind power exported into the grid (and minimising wind curtailment), the AA-based OPF with DTR and STR limits are solved separately and upper/lower bounds for the estimated total wind curtailments are plotted in Figure 10. DTR limits allows to export much more generated wind power: for a winter day, as there is no curtailment at all (high-wind and low temperature), while for a summer day, there is some curtailment (medium-wind and high temperature).

4.1.4 Comparison between AA-based OPF and MCS-based P-OPF

A probabilistic MCS-based OPF is then implemented to identify PDFs required for optimal dispatch solutions. In this MCS-based P-OPF, generated power of each WF is sampled according to distribution functions developed in [22], while loads are sampled with normal distributions, where standard deviations are estimated according to 0.95 and 0.05 quantiles in Figure 5. For each 30-minute time interval, 5,000 MCS solutions for all uncertain variables (eight WF generations and two load demands, as well as wind speeds and wind directions at OHLs) are inputted into the OPF solver.

The daily maximum and minimum wind curtailments determined by MCS-based P-OPF are compared with AA-OPF results in Figure 11, confirming that there is no curtailment for a winter day.

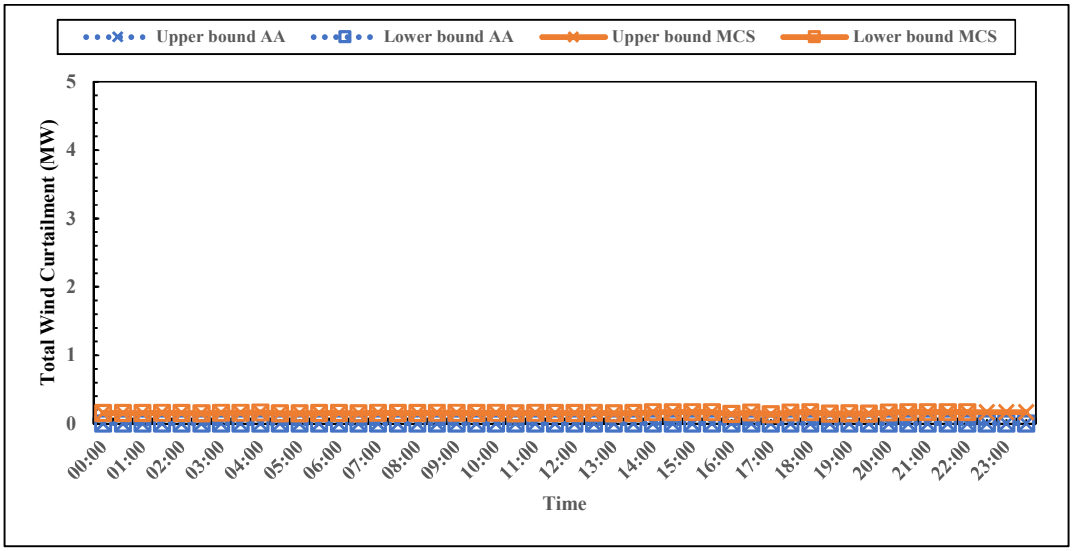

a) winter day

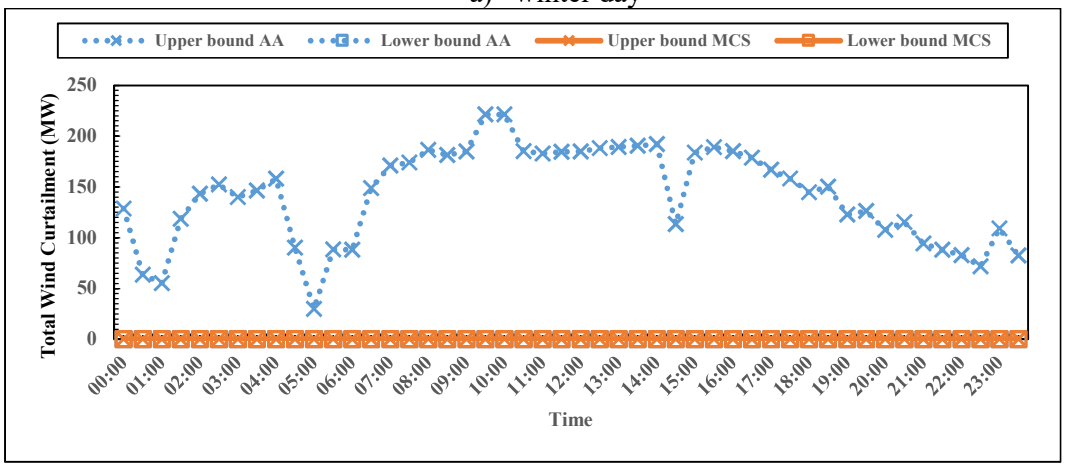

b) summer day

Figure 11. Comparison of wind curtailment results with MCS and AA methods.

For a summer day, P-OPF results give close to zero curtailment, while AA-OPF results suggest a possible large curtailment. This is because AA-OPF uses minimum and maximum values from the estimated ranges of variations, which have very low

probabilities, resulting in too large ranges of uncertainties and possible inappropriate operational decisions related to wind curtailment strategies.

To evaluate the above point in more detail, the PDFs of P-OPF solutions for wind curtailment for a summer day are plotted together with AA-OPF Min-Max intervals, and AA-OPF intervals obtained when variations of input variables are limited to their 0.05 to 0.95 quantiles uncertainty ranges in Figure 12.

At 01:00 and 05:00 hours, AA Min-Max intervals are around [0.010 MW, 55.305 MW] and [0.059MW, 29.854 MW] while 95%-5% AA intervals reduce to [0.0977 MW, 0.156 MW] and [0.085 MW, 0.164 MW]. The probability (i.e. risk) that the wind curtailment will fall out of this interval is obtained from the P-OPF distributions and in both cases is less than 0.4%. At 09:30 and 13:00 hours, Min-Max AA intervals are [0.085 MW, 221.194 MW] and [0.103 MW, 185.209 MW], while 95%-5% AA intervals reduce to [0.107 MW, 0.145 MW] and [0.106 MW, 0.147 MW] with the probability that wind curtailment will fall out of this interval less than 0.2%.

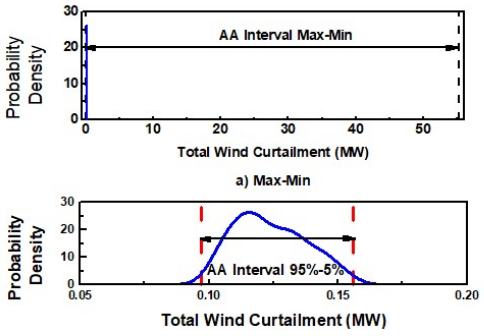

a) 01:00 hours

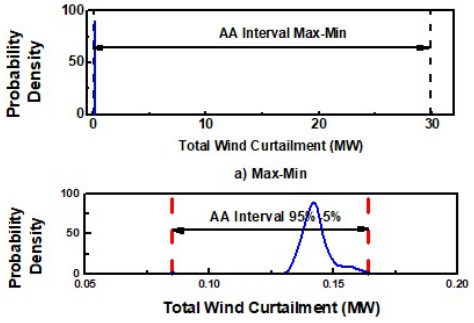

b) 05:00 hours

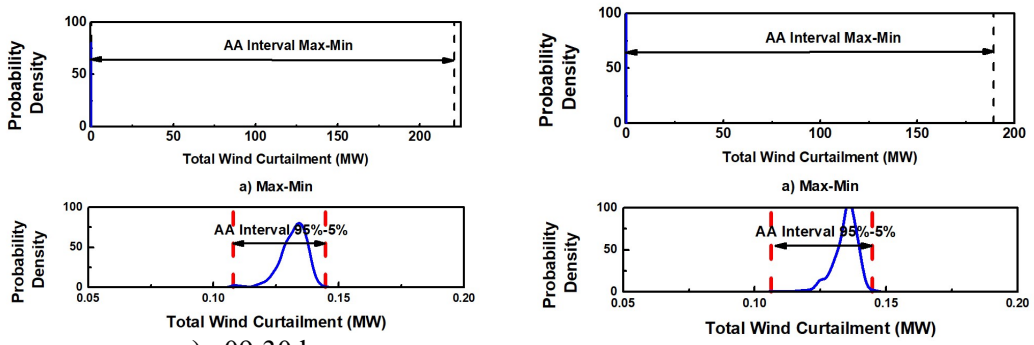

c) 09:30 hours d) 13:00 hours

Figure 12. Comparison of AA-OPF and P-OPF solutions for wind curtailment.

4.2 Case 2: 33-bus Network (Medium Size Network)

4.2.1 Network specification

In the 33-bus network, taken from [40], four WTs are located at Buses 13, 21, 24 and 29, each with rated power of 2 MW and operating with unity power factor. The total peak demand is 3.7 MW and 2.3 MVAr, which is represented with two different load profiles. The system comprises 32 transmission OHLs: DTR is applied to L1-2, which is an ACSR Fox-type conductor [35], while for other OHLs the STR of 200 A is applied. The variations in wind generation are balanced by controlling thermal generation at Bus 1. As in the previous case study, AA-OPF and P-OPF methods are used to calculate interval values and probability distributions of the WTs the power outputs, from which required thermal generation reserve for supplying variable demands can be determined. The same load profiles and wind profiles presented in Figures 5, 6 and 7 are applied to wind demands, generation and calculation of DTR of OHL.

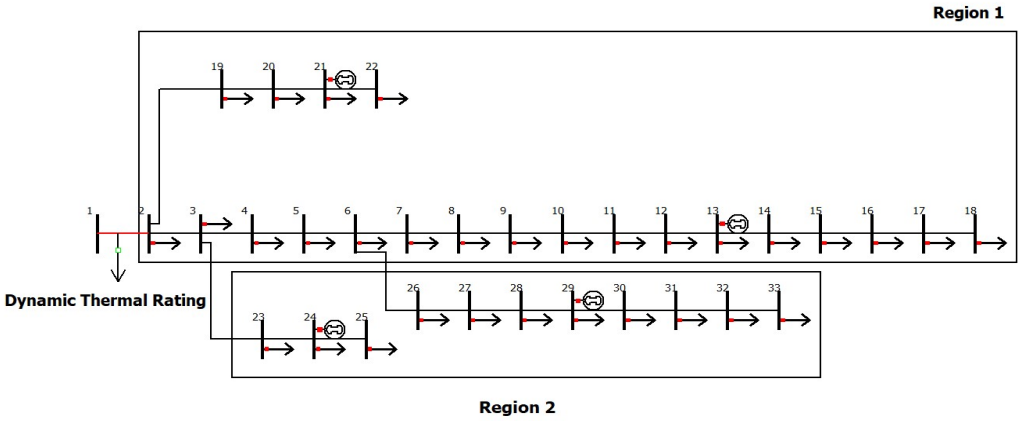

Figure 13. Configuration of the 33-bus distribution network.

4.2.2 Comparison between AA- OPF and P-OPF results

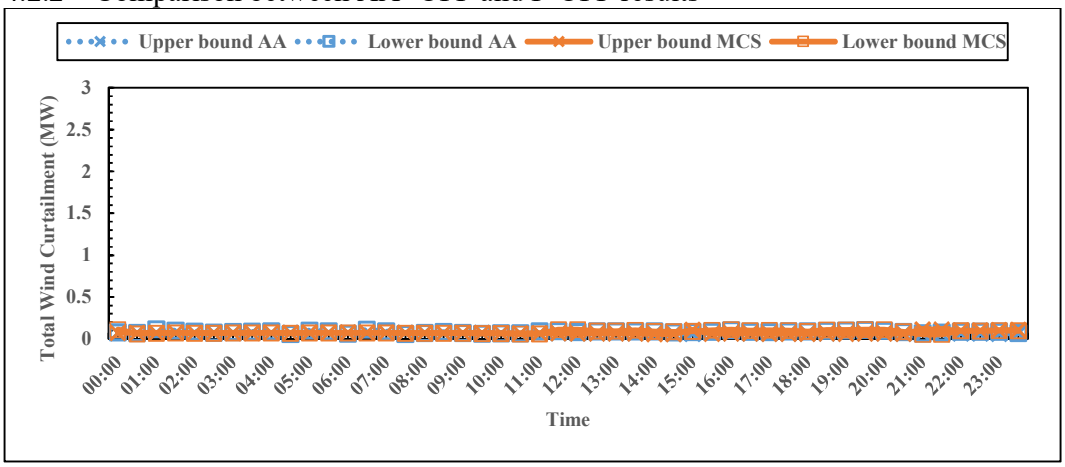

a) winter day

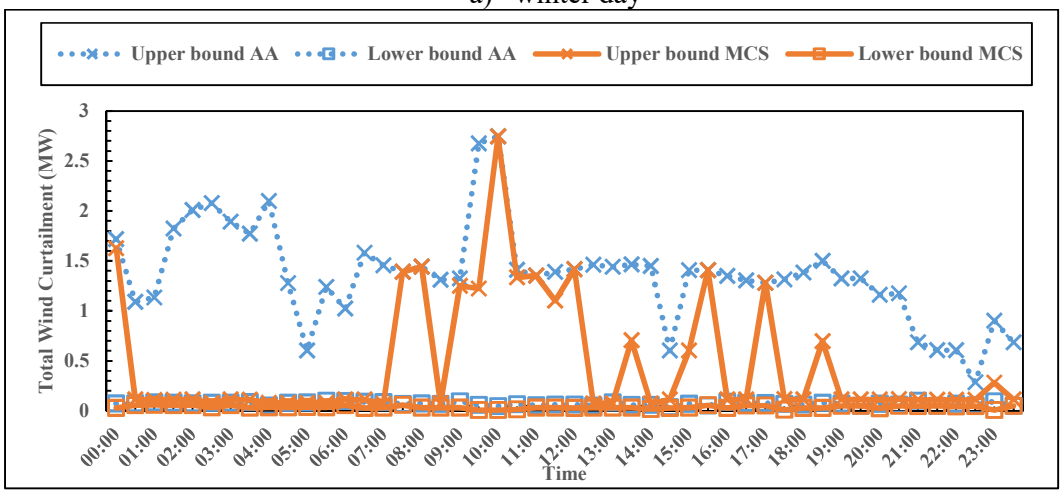

a) summer day

Figure 14. Comparison of wind curtailment results with AA-OPF and P-OPF methods.

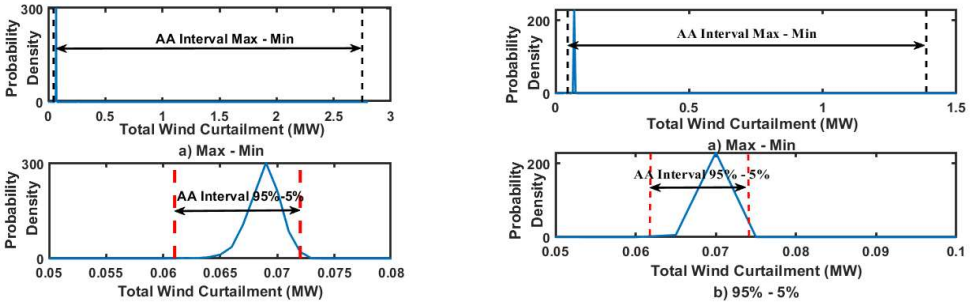

a) 10:00 hours b) 13:30 hours

Figure 15. Comparison of AA-OPF and P-OPF solutions for wind curtailment.

Maximum and minimum daily wind curtailment profiles obtained by AA-OPF and P-OPF are plotted in Figure 14, again for one day in summer and one day in winter. On the winter day, no wind curtailment is implemented, because OHL thermal rating is extended significantly when DTR is applied (low ambient temperature and high wind speed). However, during most of the time on the summer day, significant wind curtailment is required to prevent overloading, but Min-Max curtailment interval provided by AA-OPF is wider than by P-OPF method. The corresponding uncertainty ranges are detailed in Figure 15, where PDFs of P-OPF solutions at two hours on the considered summer day are plotted together with AA-OPF Min-Max intervals and 95%-5% intervals. At 10:00 hours, the curtailment value interval obtained by P-OPF method is [0.047 MW, 2.744 MW], while the Min-Max interval obtained by AA-OPF is [0.008 MW, 2.747 MW]. If again 95%-5% AA interval is used, the uncertainty in curtailed wind energy reduces to [0.060 MW, 0.072 MW] without introducing significant risk. Similar results are obtained at 13:30 hours, when Min-Max AA interval of [0.017 MW, 1.465 MW] reduces in case of 95%-5% AA interval to [0.062 MW, 0.074 MW].

The results for the analysis of the second test network also indicate that optimal generation dispatch and wind curtailment regime can be obtained if too wide solutions ranges of AA-OPF with Min-Max intervals are evaluated in terms of the involved risks

and uncertainties with the selected confidence levels. The process of finding appropriate confidence level can be denoted as a tuning of AA-OPF method and is much faster than MCS-based P-OPF approach, as it does not require large number of simulations. In other words, a limited number of selected P-OPF cases can be solved first, to assess solution intervals, confidence levels and related risks, and then AA-OPF can be used for further analysis. In that way, these two approaches will be combined in an AA-P-OPF approach, as it is presented in this paper.

5 Conclusions

A novel OPF model with probabilistic DTR limits is presented for a day-ahead planning of networks with high wind penetration. The model combines AA-OPF and P-OPF approaches and is illustrated on a case study of a real transmission network (small system) and 33-bus network (medium size system). Time series with uncertainties are generated using Copula Function and second-order MC model, based on recorded historical data. The presented AA-P-OPF method can be used by system operators for optimal generation dispatch and for selection of low-risk wind curtailment strategies, where risk level is directly related to the specified confidence level in the evaluated uncertainty ranges. Compared to the sampling-based P-OPF approach, the presented AA-P-OPF method is much more efficient in terms of the required computational times, while it can also resolve issue with too wide solution ranges obtained by AA-OPF method with Min-Max intervals, as it can take into account probability distributions of input uncertainties. A possible extension of the presented work is implementation of chance-constrained OPF analysis, which is subject of the future work by the authors.

References

[1] P. B. Eriksen, T. Ackermann, H. Abildgaard, P. Smith, W. Winter and J. M. Rodriguez Garcia, "System operation with high wind penetration," in *IEEE Power and Energy Magazine*, vol. 3, no. 6, pp. 65-74, Nov.-Dec. 2005.

[2] J. Decesaro, K. Porter, "Wind energy and power system operations : a review of wind integration studies to date," *Electr. J.*, vol. 22, no. 10, pp. 34–43, 2009.

[3] "Overhead electrical conductors - Calculation methods for stranded bare conductors," in IEC Standard 61597, 1995.

[4] "IEEE Standard for calculating the current-temperature relationship of bare overhead conductors," in IEEE Std 738-2012 (Revision of IEEE Std 738-2006 - Incorporates IEEE Std 738-2012 Cor 1-2013), vol., no., pp.1-72, 23 Dec. 2013.

[5] "The Thermal behaviour of overhead conductors - sections 1 and 2: mathematical model for evaluation of conductor temperature in the steady state and the application," in CIGRE WG 22.12, Electra. 144 (1992), pp. 107-125.

[6] A. Michiorri, "Power system real-time thermal rating estimation," Ph.D. dissertation, Dept. Eng. Comput. Sci., Durham Univ., Durham, U.K., 2010.

[7] D. A. Douglass and A. Edris, "Real-time monitoring and dynamic thermal rating of power transmission circuits," *IEEE Trans. Power Del.*, vol. 11, no. 3, pp. 1407–1418, Jul. 1996.

[8] J. Yang, X. Bai, D. Strickland, L. Jenkins and A. M. Cross, "Dynamic network rating for low carbon distribution network operation—a U.K. application," in *IEEE Trans. Smart Grid*, vol. 6, no. 2, pp. 988-998, March 2015.

[9] A. Safdarian, M. Z. Degefa, M. Fotuhi-Firuzabad and M. Lehtonen, "Benefits of real-time monitoring to distribution systems: dynamic thermal rating," in *IEEE Transactions on Smart Grid*, vol. 6, no. 4, pp. 2023-2031, July 2015.

[10] M. Z. Degefa, M. Humayun, A. Safdarian, M. Koivisto, R. J. Millar and M. Lehtonen, "Unlocking distribution network capacity through Real-time thermalrating for high penetration of DGs," in *Electric Power Systems Research*, vol. 117, pp. 36-46, Aug 2014.

[11] M. Ali, M. Z. Degefa, M. Humayun, A. Safdarian and M. Lehtonen, "Increased utilization of wind generation by coordinating the demand response and real-time thermal rating," *in IEEE Transactions on Power Systems*, vol. 31, no. 5, pp. 3737-3746, Sept. 2016.

[12] J. Cao, W. Du, H. Wang, "Weather-based optimal power flow with wind farms integration," in *IEEE Transactions on Power Systems*, vol. 31, no. 4, pp. 3073-3081, 2016.

[13] P. Zhang and S.T. Lee, "Probabilistic load flow computation using the method of combined cumulants and Gram-Charlier expansion," *IEEE Trans. on Power Syst.*, vol.19, no.1, pp. 676-682, Feb. 2004

[14] A. Schellenberg, W. Rosehart, and J. Aguado, "Cumulant-based probabilistic optimal power flow (P-OPF) with Gaussian and Gamma distributions*," IEEE Trans. on Power Syst.*, vol. 20, no. 2, pp. 773–781, May 2005.

[15] H. Zhang and P. Li, "Chance constrained programming for optimal power flow under uncertainty," *IEEE Trans. on Power Syst.*, vol. 26, no. 4, pp. 2417-2424, Nov. 2011.

[16] G. Verbic and C. A. Cañizares, "Probabilistic optimal power flow in electricity markets based on a two-point estimate method," *IEEE Trans. Power Syst*., vol. 21, no. 4, pp. 1883–1893, Nov. 2006.

[17] L. Pereira, V. Da Costa, A. L.S. Rosa, "Interval arithmetic in current injection power flow analysis," *International Journal of Electrical Power and Energy Systems,* vol. 42, pp. 1106-1113, Jul. 2012.

[18] X. Guan, W.H.E. Liu, A. D. Papalexopoulos, "Application of a fuzzy set method in an optimal power flow," *Electric Power Systems Research,* vol 34, no. 1, pp. 11-18, Jul 1995.

[19] M. Pirnia, C. A. Cañizares, K. Bhattacharya and A. Vaccaro, "A novel affine arithmetic method to solve optimal power flow problems with uncertainties," in *IEEE Trans. on Power Syst.*, vol. 29, no. 6, pp. 2775-2783, Nov. 2014.

[20] O. Bouissou, E. Goubault, J. G. Larrecq and S. Putot, "A generalization of p-boxes to affine arithmetic", in *Computing*, vol. 12, 2012.

[21] O. Bouissou, E. Goubault, S. Putot, A. Chakarov and S. Sankaranarayanan, "Uncertainty propagation using probabilistic affine forms and concentration of measure inequalities." in *International Conference on Tools and Algorithms for the Construction and Analysis of Systems*, pages 225–243. Springer, 2016

[22] D. Fang, M. Zou and S. Djokic, "Probabilistic OPF incorporating uncertainties in wind power outputs and line thermal ratings," *2018 IEEE International Conference on Probabilistic Methods Applied to Power Systems (PMAPS)*, Boise, USA, 2018, pp. 1-6.

[23] L.H. De Figueiredo, J. Stolfi, “Affine arithmetic: concepts and applications,” in *Numerical Algorithms,* vol. 37, pp147-158, 2003.
[24] J. Stolfi, L.H. De Figueiredo, “Self-validated numerical methods and applications”, Brazilian Mathematics Colloquium Monograph, IMPA, Rio De Janeiro, Brazil, 1997.
[25] A. Vaccaro and C. A. Cañizares, "An affine arithmetic-based framework for uncertain power flow and optimal power flow studies," in *IEEE Trans. on Power Syst.*, vol. 32, no. 1, pp. 274-288, Jan. 2017.
[26] S. Wang, K. Wang, F. Teng, G. Strbac and L. Wu, “An affine arithmetic-based multi-objective optimization method for energy storage systems operating in active distribution networks with uncertainties” in *Applied Energy,* vol. 223, pp. 215-228, Aug. 2018.
[27] A. Piccolo, A. Vaccaro and D. Villacci, “Thermal rating assessment of overhead lines by Affine Arithmetic,” in *Electric Power Systems Research*, vol. 71, pp. 275-283, May. 2004.
[28] G. Papaefthymiou, and B. Klockl, “MCMC for wind power simulation,” in *IEEE Trans. on Energy Conversion*, vol. 23, no. 1, pp. 234-240, 2008.
[29] Y. Pan, L. Shi, and Y. Ni, “Modelling of multiple wind farms output correlation based on copula theory,” in *The Journal of Engineering*, vol. 2017, no. 13, pp. 2303-2308, 2017.
[30] G. Papaefthymiou, and D. Kurowicka, “Using Copulas for modelling stochastic dependence in power system uncertainty analysis,” in *IEEE Trans. on Power Syst.*, vol. 24, no. 1, pp. 40-49, 2009.
[31] A. Shemyakin, and A. Kniazev, *Introduction to Bayesian Estimation and Copula Models of Dependence*, Wiley, 2017.
[32] A. Sklar, *Fonctions de répartition à n dimensions et leurs marges* [N-dimensional marginal and joint distribution functions]. Université Paris 8, 1959, pp. 229-231.
[33] British Atmospheric Data Centre. (2012) UK Meteorological Office, MIDAS land surface stations data (1853-current). [Online]. Available: http://badc.nerc.ac.uk/home/index.html.
[34] G. Coletta, A. Vaccaro, D. Villacci, D. Fang and S. Djokic, “Affine arithmetic for efficient and reliable resolution of weather-based uncertainties in optimal power flow problems,” in *International Journal of Electrical Power & Energy Systems*, vol., no., pp.1-18, Mar. 2018. *(under review)*
[35] Eland Cables, “ACSR - ASTM - B Aluminium Conductor Steel Reinforced”, Eland Technical Specification, 2017.
[36] M. Lydia, S. S. Kumar, A. I. Selvakumar, and G. E. Prem Kumar, “A comprehensive review on wind turbine power curve modelling techniques,” in *Renew. Sustain. Energy Rev*., vol. 30, pp. 452–460, 2014.
[37] M. Zou, D. Fang, and S. Djokic, "Assessment of wind energy resources and identification of outliers in on-shore and off-shore wind farm measurements," in *3rd International Conference on Offshore Renewable Energy (CORE)*, 2018.
[38] J. Fu, S. Abbott, B. Fox, D. J. Morrow and S. Abdelkader, "Wind cooling effect on dynamic overhead line ratings," *45th International Universities Power Engineering Conference UPEC2010*, Cardiff, Wales, 2010, pp. 1-6.
[39] W. Z. Black and W. R. Byrd, "real-time ampacity model for overhead lines," in IEEE Transactions on Power Apparatus and Systems, vol. PAS-102, no. 7, pp. 2289-2293, July 1983.
[40] M. E. Baran and F. F. Wu, "Network reconfiguration in distribution systems for loss reduction and load balancing," in IEEE Transactions on Power Delivery, vol. 4, no. 2, pp. 1401-1407, Apr 1989.